minerals

MDPI

Article

Thermal-Infrared Spectral Feature Analysis and Spectral Identification of Monzonite Using Feature-Oriented Principal Component Analysis

Busheng Xie [1,2], Wenfei Mao [1,2,*], Boqi Peng [1,2], Shengyu Zhou [3] and Lixin Wu [1,2]

[1] School of Geosciences and Info-Physics, Central South University, Changsha 410083, China; bushengxie@csu.edu.cn (B.X.); pengboqi@csu.edu.cn (B.P.); wulx66@csu.edu.cn (L.W.)
[2] Laboratory of Geo-Hazards Perception, Cognition and Predication, School of Geosciences and Info-Physics, Central South University, Changsha 410083, China
[3] Zhongnan Engineering Corporation Limited, Changsha 410083, China; zhoushengyu1996@163.com
* Correspondence: maowenfei@csu.edu.cn

Abstract: Rock spectral analysis is an important research field in hyperspectral remote sensing information processing. Compared with the spectra in the short-wave infrared and visible–near-infrared regions, the emittance spectrum of rocks in the thermal infrared (TIR) region is highly significant for identifying some major rock-forming minerals, including feldspar, biotite, pyroxene and hornblende. Even for the same rock type, slight differences in mineral composition generally result in varying spectral signatures, undoubtedly increasing the difficulty in discriminating rock types on the Earth's surface via TIR spectroscopy. In this study, amounts of monzonite samples from different regions were collected in the central part of Hunan Province, China, and emission spectra at 8–14 μm were measured using a portable thermal infrared spectrometer. The experimental result illustrates 13 remarkable feature positions for all the monzonite samples from different geological environments. Furthermore, by combining the extracted features with the principal component analysis (PCA) method, feature-oriented PCA was applied to establish a model for identifying monzonite accurately and quickly without performing spectral library matching and spectral deconvolution. This study provides an important method for rock type identification in the TIR region that is helpful for the rock spectral analysis, geological mapping and pixel unmixing of remote sensing images.

Keywords: thermal infrared spectra; identification model; feature-oriented PCA; monzonite

Citation: Xie, B.; Mao, W.; Peng, B.; Zhou, S.; Wu, L. Thermal-Infrared Spectral Feature Analysis and Spectral Identification of Monzonite Using Feature-Oriented Principal Component Analysis. *Minerals* **2022**, *12*, 508. https://doi.org/10.3390/min12050508

Academic Editor: Amin Beiranvand Pour

Received: 15 March 2022
Accepted: 17 April 2022
Published: 20 April 2022

1. Introduction

The spectral features of rocks are closely related to their lithology and structural features (e.g., mineral composition, particle size and porosity), and types of ground objects can be distinguished on the basis of their spectral information. Rock spectral analysis is an important research direction of hyperspectral remote sensing, which is widely used in lithology and mineral mapping in the geological field [1]. Compared with time- and resource-consuming approaches, such as X-ray diffraction analysis and inductively coupled plasma optical emission spectroscopy, the identification and analysis of rocks and minerals by using spectral information are more effective and economical [2,3]. Physically, rocks exhibit inherent spectral features due to the differences in their reflection and radiation properties at different wavelengths [4]. Electromagnetic waves with different wavelengths have varying responses to ions and atomic groups in minerals; thus, the abilities of the spectra at the visible–near-infrared (VNIR), short-wave infrared (SWIR) or thermal infrared (TIR) regions to identify different rocks and minerals considerably differ [5]. Previous studies on rock spectral analysis have mostly focused on the band at 0.38–2.5 μm, and studies on rock TIR spectral features are relatively limited. In general, the spectra of rocks at the VNIR and SWIR regions largely reflect the electron movement of metal ions and

the molecular vibrations of hydroxyl-containing minerals. Thus, oxides and hydroxides that contain transition elements (e.g., Fe and Mn), carbonate minerals and part of hydrated sulphate minerals can be identified correspondingly. Meanwhile, the TIR spectra of rocks mostly reflect the fundamental frequency of molecular vibrations, which are of good ability to identify anhydrous and hydroxyl-free minerals, such as shelf silicates, island silicates, single chain silicates, carbonates and sulphates [6,7]. Accordingly, in this paper, spectral shape in the TIR band (8–14 μm) was considered for the identification of collected igneous rock samples.

On the basis of hyperspectral technology, rock identification and classification methods currently account for two types of information: full-band information and spectral diagnostic features. The former includes the spectral angle classification method, the spectral feature fitting classification method, the binary coding method, etc., in which matching degree between the measured spectral curve of a rock and the standard rock curve in existing spectral libraries are primarily considered. Evidently, such methods rely strictly on the establishment and update of spectral libraries, such as the United States Geological Survey (USGS) [5], Arizona State University thermal emission [8], Advanced Spaceborne Thermal Emission and Reflection Radiometer (ASTER) [9], Specchio [10] and RockSL [11] spectral libraries. These libraries provide a large amount of standard spectral data and remote sensing image extraction of spectral endmembers. Govil et al. [12] extracted chlorite, muscovite, illite and goethite in the Kuta region of the Indian Himalayas by using the spectral angle classification method, which provides important information for mineral exploration in regions with complex landforms. Using the same method, Rezaei et al. [13] drew a lithology map of the Sangan area in northeastern Iran based on ASTER images and USGS spectral database data, with an accuracy of 79% compared with field investigation data. However, lithological classification and field verification are typically not completely matched in previous studies, and the possible reasons are as follows: (1) the error caused by the accuracy of the applied matching algorithm; and (2) for a given rock type, different geological and diagenetic environments slightly affect the rock's compositions and structures, and the corresponding spectral features differ to a certain extent. However, spectral data in a spectral library are generally based on the laboratory measurement of pure materials, which may considerably differ from the studied objects [1]. Moreover, the accuracy of spectral matching technology based on full-band information relies on spectral pixel unmixing, and thus, spectral information extracted from mixed pixels frequently leads to the unreliability of spectral matching results.

To solve the aforementioned problems, the analysis of diagnostic features based on spectral curves was proposed and developed. The principle of this method is to extract features from a spectral curve that contains redundant information or compress spectral curve information by reducing its dimensions, such as principal component analysis (PCA), and consequently, rocks and minerals can be identified on the basis of the extracted parameters. For example, Loughlin [14] studied rock alteration information from extracted spectral features by using PCA. By combining PCA with the wave band ratios of TM5/TM7 and TM3/TM1 (TM1, TM3, TM5 and TM7 represent different bands of Landsat images), Rokos et al. extracted the alteration information of low-temperature hydrothermal Au deposits in the Quaternary Island arc of the Aegean Basin [15]. Xie et al. [16] extracted the spectral features of limonite (Fe^{3+}), chlorite (Mg-OH group minerals) and kaolinite (Al–OH group minerals) and further extracted mineral alteration information by combining with PCA. However, in terms of full-band information that contains considerable redundant information, dimension-reducing processing based on the subjective selection of feature bands or the use of the PCA algorithm leads to unreliable rock classification results to a certain extent, and thus, the procedure should be improved further.

The mineral composition and structure of exposed rocks in the central part of Hunan Province, China, are diverse and complex due to volcanic and tectonic activities. Therefore, analysing remote sensing images accurately and quickly by using traditional spectral analysis algorithms is extremely difficult. Considering the potential applications of the TIR

spectroscopy of rocks in the fields of land use survey [17,18], lithology mapping [19–21] and mineral prospecting [22,23], our team went to the central part of Hunan Province in 2019 to conduct field geological survey and rock sampling. In this paper, the TIR radiation spectra of 19 monzonite samples collected from different regions were measured, and the corresponding features were analysed. On the basis of the extracted common spectral features of different monzonite samples, an identification model of monzonite was established by combining with PCA, and the objective of identifying monzonite samples effectively and accurately was realized.

2. Materials and Method

2.1. Description of Sampling Sites

Longhui County is located at the northern part of central Hunan Province, China, which extends from 110°44′0″ to 111°16′0″ E longitude and from 27°26′0″ to 27°42′0″ N latitude, covering an area of about 2496 km^2 (Figure 1a). The central Hunan Province, located in the metamorphic belt of the Caledonian age, is not only a region of Yangzi igneous rock but also of Yunkai–Hainan igneous rock [24]. The sampling area is located at a down warping region in the Qiangtang–Yangzi–Huanan block, and geological ages range from the Cretaceous and the Jurassic to the Silurian. The major faults in the geological structure lie between the Jiangkou–Wutuan fault and the Xinhua–Chengbu fault, extending from the south to the north [25]. Moreover, this county is abundant in mineral resources, particularly monzonite, and has a hilly terrain. Considering its diversity and complexity in geological structure, this region was selected as the study area, and it is shown in detail in Figure 1b.

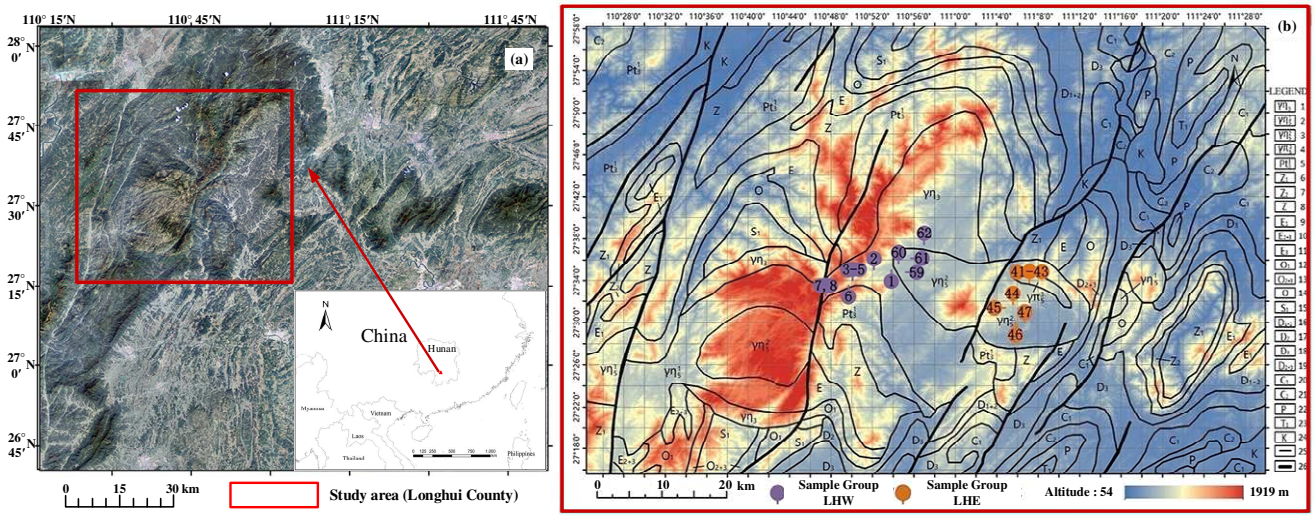

Figure 1. Geographical location of the research area and distribution of rock sampling points: (**a**) location of research area and (**b**) geological structure, lithological distribution and rock sampling points in the central area of Hunan Province, China. The samples were classified into two groups on the basis of their sampling position. Legend: 1: Silurian. 2: Triassic. 3: Jurassic. 4: Cretaceous. 5: Upper Proterozoic. 6–8: Sinian. 9–11: Cambrian. 12–14: Ordovician. 15: Silurian. 16–19: Devonian. 20, 21: Carboniferous. 22: Permian. 23: Triassic. 24: Cretaceous. 25: Boundary of strata. 26: Faults.

2.2. Rock Sampling

From July to April in 2020, the team investigated the geological environment and sampled crude rocks in this area. A total of 65 rock samples, exposed on the land surface, were collected from the study area. In accordance with the geological map published by the Institute of Geology of the Chinese Academy of Geological Sciences and visual interpretation during field investigation, 19 rock samples were preliminarily identified as monzonite, selected to undergo spectrum test and further authenticated through thin sections (Figure 2). These rock samples were mostly derived from three geological ages,

namely, Cretaceous, Jurassic and Silurian, on the basis of the relationship of sampling positions and the geological map of Hunan Province.

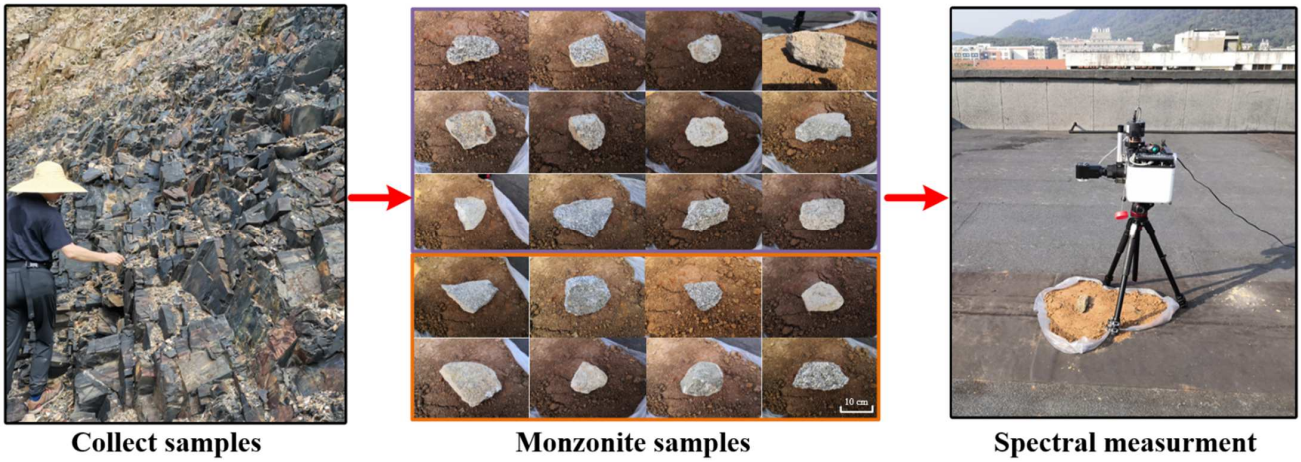

Figure 2. Process of spectral data collection.

In accordance with the spatial distribution of sampling points, the rock samples were divided into two groups to facilitate further analysis. The Longhui western (LHW) group was located at the western side of the sampling area, whilst the Longhui eastern (LHE) group was located at the eastern side of the sampling area (Figure 1b). The LHW group includes three rock samples from the Cretaceous and nine rock samples from the Silurian. The LHE group comprises eight rock samples, with the former four belonging to the Cretaceous and the latter four to the Jurassic.

To acquire further information on the rock samples, we conducted identification, which suggest that the rock samples were definitely monzonite, in accordance with the thin sections observed using a professional microscope Axioskop 40 (Carl Zeiss, Jena, Germany). Selected from all the thin sections, two sections (LH42 and LH61) were calibrated as standardized examples that comprised K-feldspar, plagioclase, biotite, hornblende and quartz in major (Figure 3a) and clay minerals, chlorite and epidote in minor (Figure 3b).

2.3. Spectroscopic Measurements

In this study, we used a portable Fourier transform TIR spectrometer 102 F produced by D&P Inc. (Hartford County, CT, USA). It can survey radiation brightness, emissivity and temperature and can calculate reflection and absorption to test the spectrum properties of all the samples. The spectral range of this instrument is 2–16 μm, with a resolution of 4 cm^{-1}. Spectral accuracy is ±1 cm^{-1}. In addition, the field angle is 4.8°, and instrument internal temperature ranges from 288 K to 308 K.

We tested all the samples on an empty roof at Yuelu Mountain in Changsha, Hunan Province, with unveiled sky and steady sunshine (Figure 2). Environment temperature was around 296.16 K, and relative humidity ranged from 20% to 50%. Furthermore, the angle of the sun's altitude was greater than 40°. In spectral measurement, the distance between the lens and the sample was about 1.0 m, and sampling integral time was set to 3 s. To weaken the disturbance caused by different directions in the spectrum test, all the samples were rotated at different angles, including 0°, 90°, 180° and 270°, to be surveyed two times by each angle. The mean of all emissivity curves was used as spectral data to ensure the stability and representativeness of the spectrum curves.

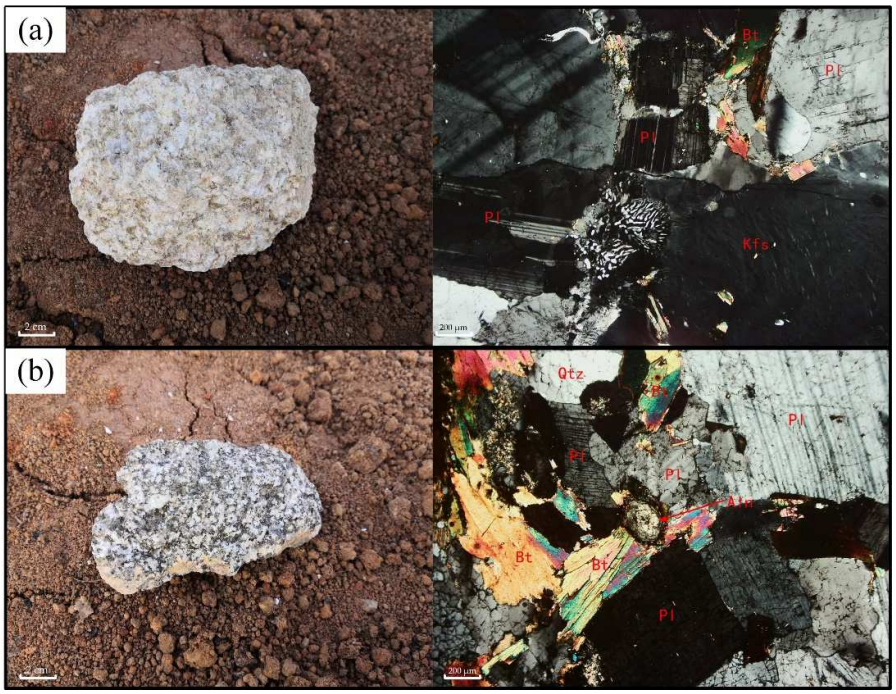

Figure 3. Result of thin section identification. The result indicates the following mineral components: plagioclase (PI), K-feldspar (Kfs), biotite (Bt), quartz (Qtz) and epidote (Aln). (**a**) Rock sample LH42 (from Cretaceous). (**b**) Rock sample LH61 (from Jurassic).

2.4. Method

2.4.1. Data Preprocessing

The infrared information of rocks at room temperature (around 293.16 K) is concentrated at the corresponding region of 3–18 μm. Moreover, the wavelength position around 10 μm in the TIR region is the most sensitive to the spectral radiation feature of rocks on Earth surface [26,27]. The TIR spectral information in some bands (between 3 μm and 7 μm and after 15 μm) was considerably affected by water vapour and carbon dioxide in the atmospheric environment. To avoid the influence of the environment, this study eliminated the noise spectral bands described above and selected a stable region (8–14 μm) with high signal-to-noise ratio (valuated by a root-mean-square error of about 0.05) for research.

To enhance the features of rock TIR spectra, the continuum removal algorithm was used to preprocess all the spectral curves [27]. The continuum removal process has two steps. (1) All the maximum points (local maximum) on the spectral curve are obtained by derivation. Then, all the values are compared to obtain the maximum point (global maximum) of the target spectral curve. Subsequently, the spectrum is divided into two segments on each side of the global maximum and treated independently. (2) The maximum point (global maximum) is taken as an endpoint of the envelope. The slope of the line that connects this point and each maximum (local maximum) at the right and left sides is calculated. Subsequently, the point with the maximum slope is taken as the next endpoint of the envelope. Then, this point is used as the new starting point to cycle until the last point. The curve formed by these endpoints is an envelope (Figure 4). The features of the spectral curve can be stressed by calculating the ratio of the original emissivity curve to the envelope of each band.

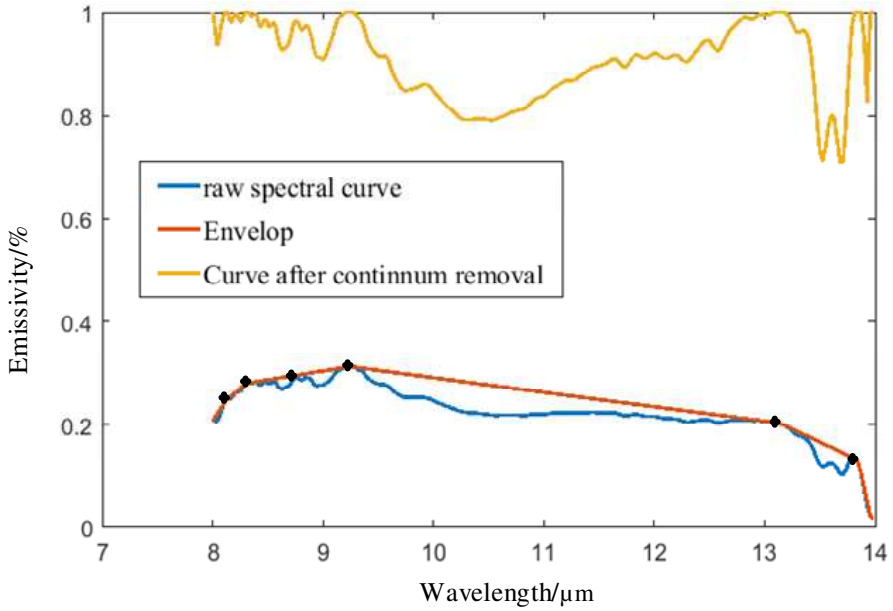

Figure 4. Illustration of continuum removal.

2.4.2. Spectral Feature Analysis

Spectral parameters, such as wavelength position, depth, width and absorption symmetry, are extracted from each spectral band after continuum removal. The definition of the feature parameters is provided in Figure 5. Symmetry is calculated by the ratio of the left and right areas of the spectral feature. The structure and band shape of each spectral feature can be accurately depicted by the combination of these parameters. Considering the mineral component and structure, each emission spectrum typically has multiple features (i.e., emission minima and maxima). Therefore, the depth parameters of the multiple emission minima of each spectrum curve are adjusted to obtain the relative depth on the basis of the normalization method for reducing interference caused by different environment conditions (e.g., light and temperature). Accordingly, the radiance information from key mineral components can be emphasized to enhance the ability of rock identification. The calculation formula describing the relative depth of emission minima in the spectral curve is as follows:

$$H = d\rho_L + (1 - d)\rho_R - \rho_0 \quad (1)$$

$$d = (\lambda_0 - \lambda_L)/(\lambda_R - \lambda_L) \quad (2)$$

$$H_{Re} = (H - H_{min})/(H_{max} - H_{min}) \quad (3)$$

where

ρ_L = the emissivity of the left endpoint of the emission spectral minima;
ρ_R = the emissivity of the right endpoint of the emission spectral minima;
ρ_0 = the emissivity of the emission minima;
λ_0 = the wavelength position of the emission minima;
λ_L = the wavelength values of the left endpoint of the emission minima;
λ_R = the wavelength values of the right endpoint of the emission minima;
H_{max} = the maximum depths of multiple emission features in the same spectral curve;
H_{min} = the minimum depths of multiple emission features in the same spectral curve.

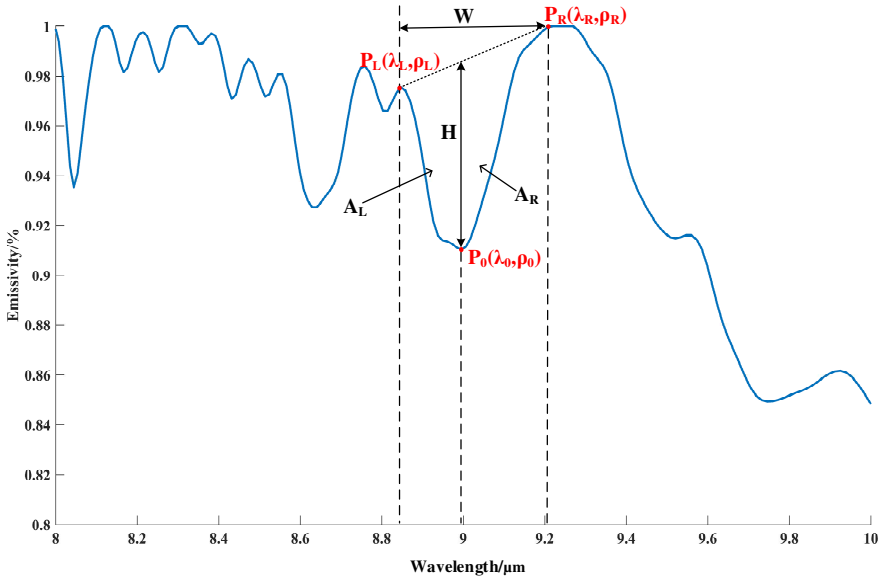

Figure 5. Quantitative parameters of the spectral feature. The red variables indicate the wavelength positions and corresponding emissivity of the emission minimum point (P_0), the left and right endpoints (P_L and P_R). H is the depth of the emission minima. W is the feature width of the emission minima.A_L and A_R are the left and right areas of the spectral feature, which can be used to calculate the symmetry of the spectral feature.

2.4.3. Establishment of the Model

After preprocessing and extracting the spectral features of the emission spectra, common and similar features were subsequently acquired from different monzonite samples with varying mineral compositions. The sensitivity analysis of three feature parameters (relative depth, width and symmetry) was performed to determine the most representative parameters for spectral identification. On the basis of the sensitive parameters of multiple common features, PCA was conducted to establish the corresponding model. Featured-oriented PCA, as a modification of the traditional PCA method, is primarily used for data compression or dimension reduction. Featured-oriented PCA gives more attention to utilising the dominant information instead of all original information before principal component transformation. To transfer all original information to several principal components representing dominant and useful information, the method makes the principal components irrelevant through orthogonal linear transformation and reduces the total amount of data information [28]. This method firstly calculates the correlation coefficient matrix of all information (e.g., full-band information of the emission curve) and then obtains the eigenvalues of the matrix (arranged from large to small) and eigenvectors. Finally, the contribution rate and cumulative contribution rate of each vector are calculated. When cumulative contribution reaches about 80%, the first few components can represent most of the information. To prove the identification accuracy and reliability of the model established using featured-oriented PCA, verification is performed by adding two monzonite samples and three non-monzonite samples (i.e., shale, mudstone and slate) to other sampling sites in the study area. The overall workflow of building the model is shown in Figure 6.

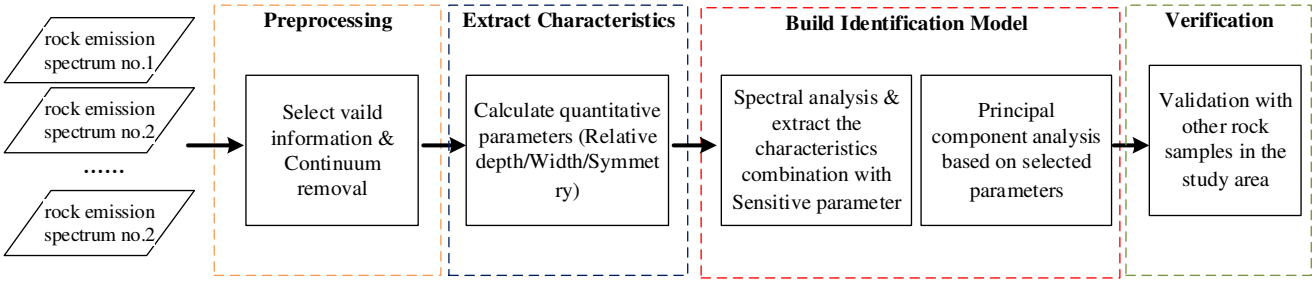

Figure 6. Workflow of model establishment and verification.

3. Results and Discussion

3.1. Features of Emission Spectrum

As the two major minerals of monzonite, plagioclase ($Na[AlSi_3O_8]$-$Ca[Al_2Si_2O_8]$) and K-feldspar ($K[AlSi_3O_8]$), play an important role in the thermal spectroscopy features of the sample spectra. Plagioclase is classified as albite, oligoclase, andesine, labradorite, bytownite and anorthite in mineralogy, while mainly includes microcline and orthoclase [29]. The fundamental frequency vibration of the Si_nO_k atomic group of primary mineral composition can be detected as evident features in the TIR spectral band. The results of the TIR emission spectra of the monzonite samples in this study are presented in. Considering the different geographical locations and geological conditions of the sampling sites, which may affect the rock emission spectrum, the spectral measurement results of the LHW group and LHE group samples described earlier are shown in Figure 7a,b, respectively. Although the emissivity intensity of the measured spectra in the LHE group is lower than that in the LHW group on the whole, the TIR emission spectra features of the two groups are basically similar. Most spectra features of the samples are consistent with the reference spectrum in the Johns Hopkins University spectral library [30] (Figure 7c). Firstly, strong minima of emission waveform ranging from 8 μm to 9 μm are present. They are mostly influenced by plagioclase and K-feldspar (major mineral content) with evident reflection peak features in the corresponding wavelength position. In addition, the weak minima and maxima of the emission spectra at around 8.7 μm may be attributed to spectral radiation features from the quartz and hornblende contents of monzonite. The strong minima and weak maxima of the emission waveform between 9 μm and 10 μm are also related to the spectral radiation features of feldspar minerals and biotite in monzonite. The emission minima between 9.2 μm and 9.3 μm exhibit a certain positive correlation with spectral features of plagioclase and biotite, while the weak emission minima of 9.5–9.7 μm are controlled by two feldspar mineral compositions. Secondly, the weak emission minima at around 12.0 μm may be caused by the orthoclase spectrum, which exhibits similar emission features in related positions. The continuous features (emission minima and maxima) between 12.3 μm and 12.8 μm are mostly affected by the plagioclase composition of monzonite. In addition, the strong emission peak (13.5–13.7 μm) and weak emission minima (around 13.8 μm) of the monzonite spectra in the 13–14 μm band may be due to the combined effects of plagioclase and biotite.

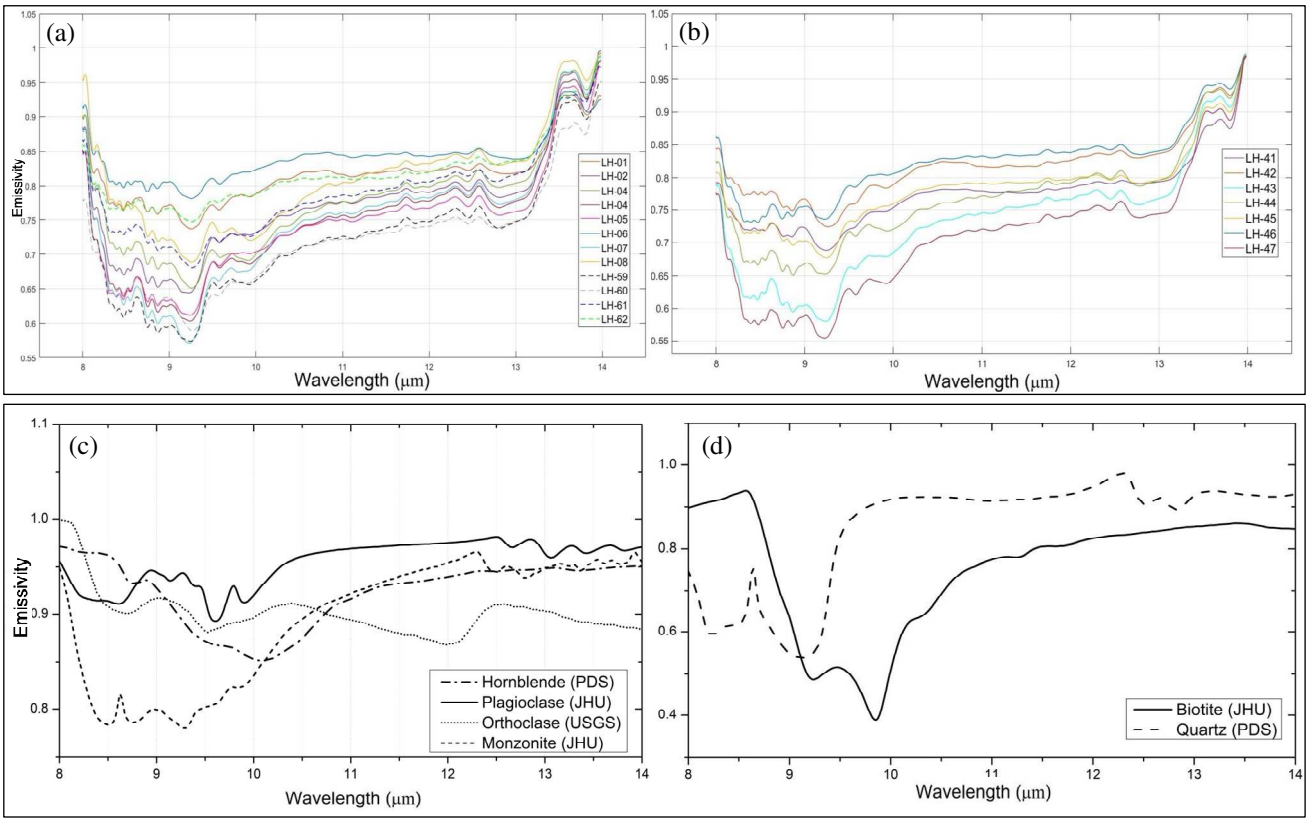

Figure 7. Rock sample emissivity curves. (**a**) LHW sample group. (**b**) LHE sample group. (**c**) Reference spectra of monzonite and pure minerals in spectral libraries, including hornblende, plagioclase and orthoclase. (**d**) Reference spectra of biotite and quartz from spectral libraries.

On the basis of the spectral analysis algorithm mentioned earlier, features with a certain wavelength position of the emission spectrum curve of 17 monzonite samples (2 monzonite samples, i.e., LH5 and LH6, were used for subsequent model verification calculation) were extracted to explore the representative and highly similar spectral emission valley position. As shown in Figure 8, the monzonite samples have common and similar features of 8.39, 8.56, 8.76, 9.28, 9.50, 11.62, 11.84, 12.0, 12.20, 12.47, 12.81, 13.6 and 13.82 μm. This finding is basically consistent with the features of the multiple emission valleys described earlier. The wavelength position and mineralogical attribution of the selected spectral features are listed in Table 1. Furthermore, to improve the accuracy and reliability of the identification model based on TIR spectroscopy, the sensitivity to common spectral information of three feature parameters (i.e., relative depth, relative width and symmetry) were comprehensively considered to establish an identification model of monzonite. Higher sensitivity indicates that the parameter values at different bands of all different samples are closer. The point density method is used to calculate the number of feature points contained in each feature point within its $0.1 \times 0.1 \times 1$ stereoscopic window in customized space with three dimensions (relative depth, width and symmetry) to obtain the density distribution of 3D feature space (Figure 9). The distribution of points with the parameters as the coordinates of the 13 extracted features shows that the features of the sample spectra are most concentrated in the relative depth at multiple feature positions. In addition, the curve showed at the bottom left panel in Figure 9 that represents the number of points close to the mean in individual dimension (1-D) of the parameters indicates that most features are dispersed in the width and symmetry dimensions, without an evident aggregation effect. The relative depth value is the most sensitive parameter, and it is associated with mineral content. Thus, it is selected alone to build the monzonite identification model without considering the other two parameters to prevent identification confusion.

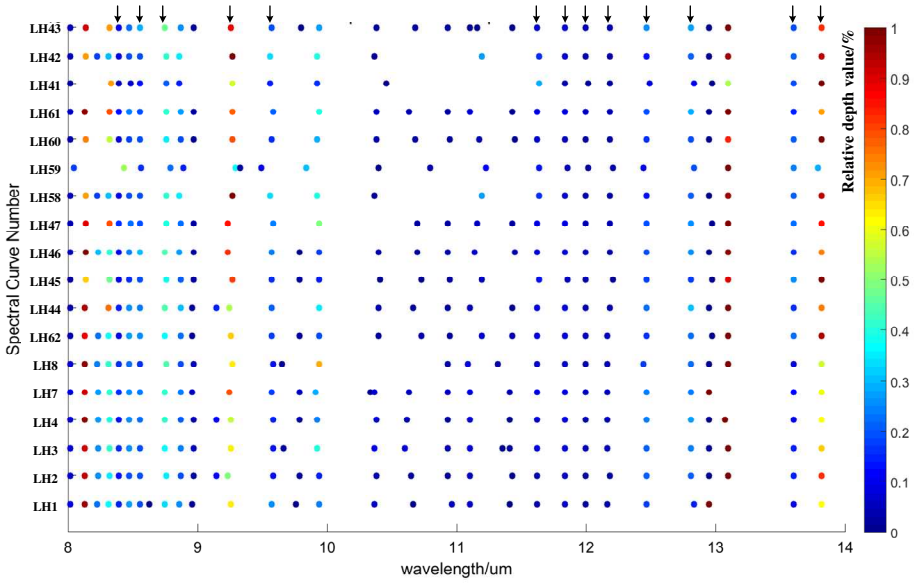

Figure 8. Distribution of the common spectral features of the monzonite samples. The colour of points represents the depth values of the extracted features. The arrows are used to point out the common and similar spectral features of the monzonite samples.

Table 1. List of selected spectral features for the identification model of monzonite

Spectral Position (μm)	Range (μm)	Mineralogical Attribution
8.39, 8.56, 8.76	8–9	quartz and hornblende
9.28, 9.50	9.2–9.3/9.5–9.7	feldspar and biotite
11.62, 11.84	11–12	/
12.0, 12.20, 12.47, 12.81	12.3–12.8	orthoclase and plagioclase
13.6, 13.82	13.5–13.7/13.8	plagioclase and biotite

3.2. Model Establishment and Verification

The PCA algorithm was implemented for the feature matrix from the relative depth parameters of multiple monzonite emission spectra to reduce the dimensions of feature space. The correlation coefficient matrix of selected parameter (i.e., relative depth) of spectral features was used for obtaining the eigenvalues and eigenvectors of the matrix. Table 2 provides the principal component eigenvalue results of the relative depth feature matrix via a linear algebra method, in which three components (i.e., PC1, PC2 and PC3) represent about 75% of the information of the overall variable. The reduction features covering most of the information of the eigenvalue matrix were applied to model establishment. The eigenvectors of the first three principal components that indicated the weights at different band positions were used to reduce feature dimension by weighting and summing the relative depths of multiple features. Based on the diagram of component eigenvectors (Figure 10), the meanings of three components (PC1, PC2 and PC3) can be further explained. Except for the first feature band, the weights of the principal component vector of PC1 in other feature bands remained stable and positive, indicating that the PC1 component, as the weighted values of the remaining bands, can reflect the overall information of the feature matrix. The principal component vector of the PC2 component has greater weight in the four features within the range of 12.5–14 μm, which is mainly due to the diagnostic spectral emission features affected by plagioclase and biotite in the monzonite samples. Therefore, the PC2 component focuses on the feature information of plagioclase and biotite in monzonites. The features of specific feature positions (11.62, 13.6 and 13.82 μm) were emphasized with the eigenvector of the PC3 component, which highlighted the diagnostic emission minima of plagioclase, biotite and possibly other trace mineral composition.

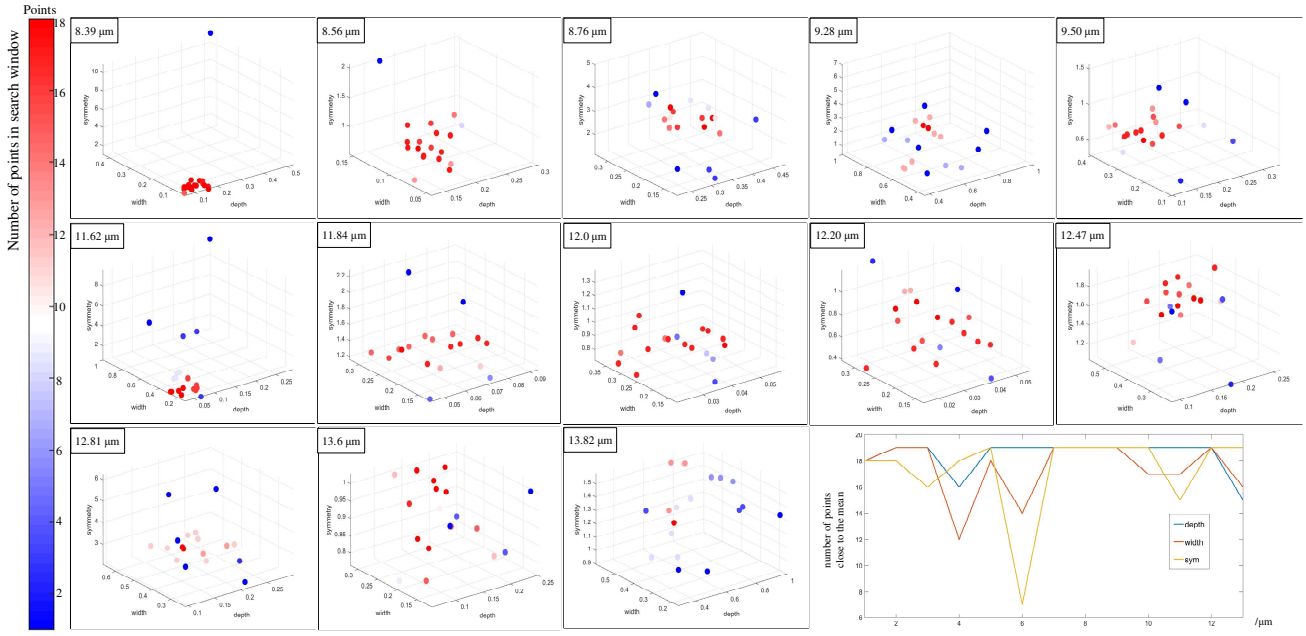

Figure 9. Distribution of each spectral feature with 19 monzonite spectra in customised space, which is described by three quantitative parameters (i.e., relative depth, width and symmetry). In other words, each point in customized space represents the array of parameters (relative depth, width and symmetry) of the emission feature of the related sample. The curves in the bottom left panel represent the number of points close to the mean in individual dimension of the parameters in all spectral features.

Table 2. Eigenvalues and cumulative variance of the correlation matrix

Component	Eigenvalue	Variance Contribution (%)	Cumulative Contribution (%)
PC1	4.5979	0.3537	0.3537
PC2	3.0972	0.2382	0.5919
PC3	2.0207	0.1554	0.7474

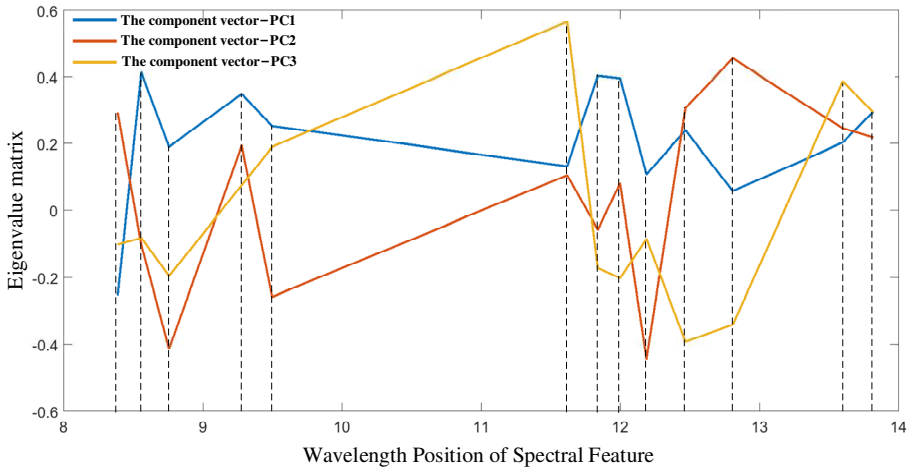

Figure 10. Eigenvectors of the first three principal components.

Building an identification model of monzonite based on the eigenvectors of the first three principal components not only emphasizes the overall feature information but also highlights the features of important mineral components. Thus, it can be proven to be scientific and reliable. Based on the feature matrix (relative depth value of the correspond-

ing wavelength position) extracted from the emission spectra of the 17 existing monzonite samples, the vector matrix of the principal components (i.e., PC1, PC2 and PC3) were obtained. In this study, the eigenvectors were used to obtain the matrix of the principal component values of 17 emission spectra (the size of the component value matrix was 17×3), and finally, calculate the average value of all principal components $(A_{PC1}, A_{PC2}, A_{PC3})$ and mean square errors $(\sigma_{PC1}, \sigma_{PC2}, \sigma_{PC3})$. The mean and triple median error of the three principal components of multiple monzonite spectra can be considered the centre coordinates and the maximum distance from the centre of the category of monzonite, respectively. In general, the model includes three steps: (1) Extracting the relative depth value of the feature position of an unknown rock sample x by means of spectral preprocessing and spectral feature analysis, and finally obtaining the depth value vector $\left(x^{(1)}, x^{(2)}, \ldots, x^{(13)}\right)$. The relative depth value is set to 0 by default when the unknown spectrum lacks an emission band at a certain feature position. (2) Calculating the three principal component values $(x_{PC1}, x_{PC2}, x_{PC3})$ of the emission spectrum of an unknown rock sample by using the feature eigenvectors shown in Figure 9. (3) Calculating the Euclidean distance amongst the three components of the unknown spectrum and the category centre $(A_{PC1}, A_{PC2}, A_{PC3})$ and judging whether the rock sample belongs to the monzonite category in accordance with the principle of triple medium error. In other words, if the distance is greater than the triple medium error, then the unknown sample is classified out of the category of monzonite; otherwise, the sample is monzonite.

To verify the reliability and usability of the identification model, two monzonite samples (LH5 and LH6) and three other rock samples from different sampling points, namely, shale (LH30), mudstone (LH38) and slate (LH53), were used for TIR spectroscopy testing and comparison (Figure 11). As shown in Figure 11, the measurement sample spectra exhibit high similarity in waveforms, making accurately identifying monzonite based on the spectral matching method difficult with the full-band spectral information. Three components (PC1, PC2 and PC3) and two components (PC1 and PC2) were used to construct a customized feature space to verify the model. The verification results are presented in Figure 12. Based on the identification model, the mudstone, shale and slate samples can be evidently eliminated, which are far from the centre of the category of monzonite, whilst the two monzonite samples (LH5 and LH6) were clearly identified. Our model can be proven to accurately distinguish monzonite from non-monzonite. The identification result of monzonite shows that the feature-oriented PCA method can effectively and accurately recognize target rock types without using spectral libraries and performing spectral unmixing, which can help related researchers to develop a similar identification model for other mineral and rock samples. Accordingly, this work initially developed a quick and reliable approach for achieving geological mapping through remote sensing observation, providing a reference for applications to geological remote sensing and planetary missions.

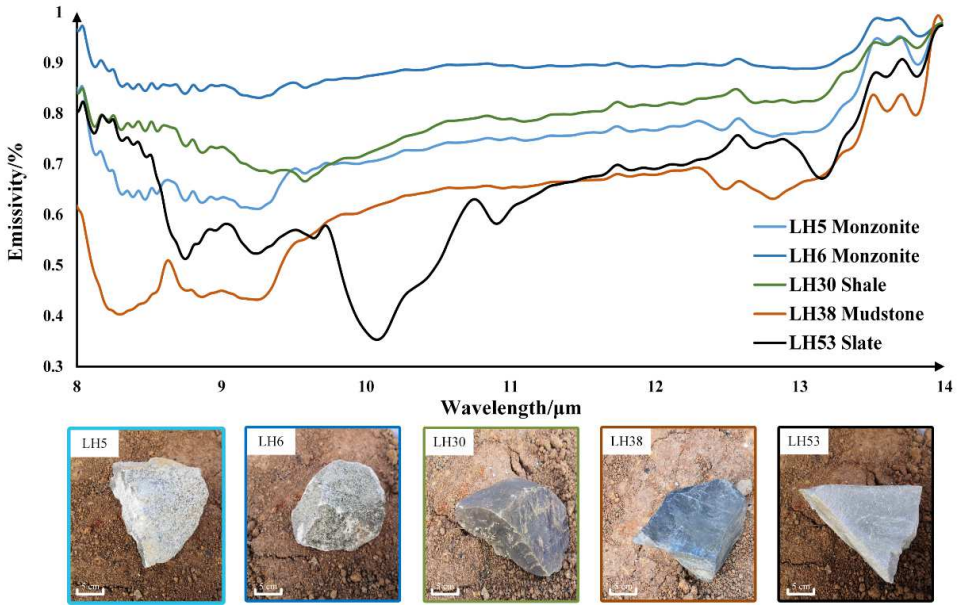

Figure 11. TIR spectral curves and optical images of samples for model verification.

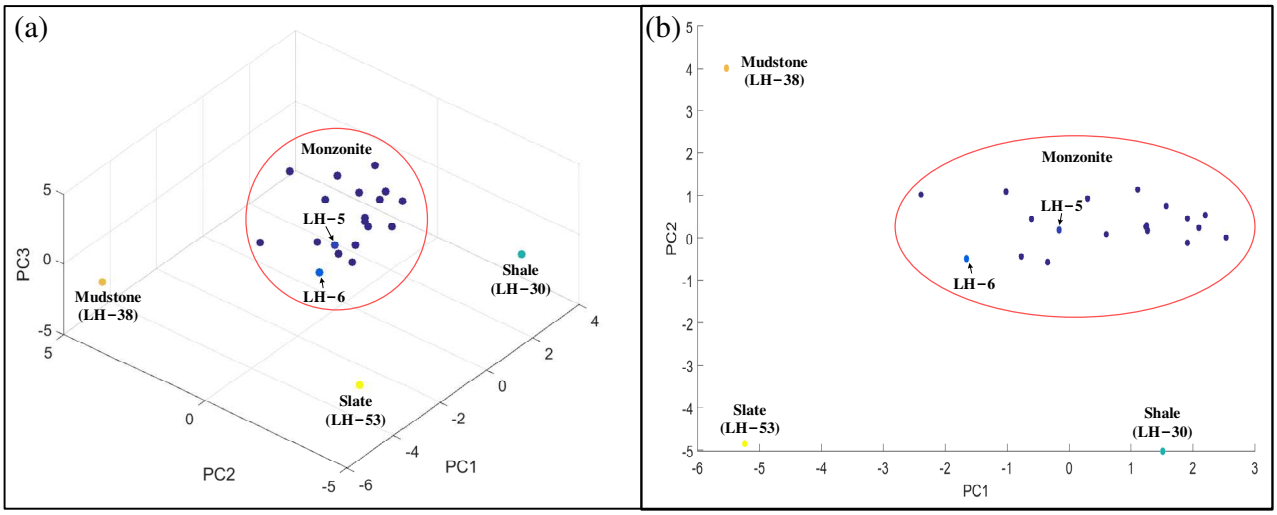

Figure 12. Results assessed by identification model: (**a**) verification result in 3D space (PC1-PC2-PC3), (**b**) verification result in 2D space (PC1-PC2).

4. Conclusions

In this study, the TIR spectroscopy (8–14 μm) of monzonite samples collected from different geological environments in the central Hunan Province, China, was measured and analysed. To prevent recognition deviations in full spectrum matching and reduce the influence of redundant information, the sensitivity of three parameters, i.e., relative depth, width and symmetry of the extracted emission features, was analysed. The value of relative depth is the most relevant parameter for featuring the emission spectrum of the monzonite samples. Thereafter, the traditional PCA method was utilised, and the dimensions of the feature matrix of the sensitive parameters were reduced correspondingly. Consequently, an effective and accurate identification model for monzonite was established. This study is highly significant for reducing matching errors in the geological mapping and pixel unmixing of remote sensing images.

Author Contributions: Conceptualization, L.W., W.M. and B.X.; methodology, B.X.; software, B.X.; validation, W.M.; formal analysis, W.M.; investigation, B.X.; resources, S.Z. and B.P.; data curation, W.M. and B.P.; writing—original draft preparation, B.X., W.M. and B.P.; writing—review and editing,

W.M. and L.W.; supervision, L.W.; funding acquisition, W.M. and L.W. All authors have read and agreed to the published version of the manuscript.

Funding: This research was supported by the NSFC Basic Science Center Project on theory and application of resource and environment management in the digital economy era (72088101), the Key Program of National Nature Science Foundation of China (41930108), National Nature Science Foundation of China (42101394), Project funded by China Postdoctoral Science Foundation (2021M693550), Nature Science Foundation of Hunan (2021JJ40725).

Data Availability Statement: Not applicable.

Acknowledgments: We would like to thank the providers and institutions of spectral data, including the National Aeronautics and Space Administration (PDS3 data set), the United States Geological Survey (USGS spectral library), Johns Hopkins University (JHU spectral library). Open source shared spectral data are an important foundation and content of our work.

Conflicts of Interest: The authors declare no conflict of interest.

References

1. Feng, J.; Rivard, B.; Rogge, D.; Sánchez-Azofeifa, A. The longwave infrared (3–14 μm) spectral properties of rock encrusting lichens based on laboratory spectra and airborne SEBASS imagery. *Remote Sens. Environ.* **2013**, *131*, 173–181. [CrossRef]
2. Okada, N.; Maekawa, Y.; Owada, N.; Haga, K.; Shibayama, A.; Kawamura, Y. Automated Identification of Mineral Types and Grain Size Using Hyperspectral Imaging and Deep Learning for Mineral Processing. *Minerals* **2020**, *10*, 809. [CrossRef]
3. BSchulz, G.; Merker, G.; Gutzmer, J. Automated SEM Mineral Liberation Analysis (MLA) with Generically Labelled EDX Spectra in the Mineral Processing of Rare Earth Element Ores. *Minerals* **2019**, *9*, 527. [CrossRef]
4. Michalski, J.; Kraft, M.; Sharp, T.; Christensen, P. Effects of chemical weathering on infrared spectra of Columbia River Basalt and spectral interpretations of martian alteration. *Earth Planet. Sci. Lett.* **2006**, *248*, 822–829. [CrossRef]
5. Clark, R.; Swayze, G.; Livo, K.; Kokaly, R.; Sutley, S.; Dalton, J.; McDougal, R.; Gent, C. Imaging spectroscopy: Earth and planetary remote sensing with the USGS Tetracorder and expert systems. *J. Geophys. Res. Planets* **2003**, *108*, E12. [CrossRef]
6. Meer, F.; Werff, H.; Ruitenbeek, F.; Hecker, C.; Bakker, W.; Noomen, M.; Meijde, M.; Carranza, E.M.; Smeth, J.; Woldai, T. Multi-and hyperspectral geologic remote sensing: A review. *Int. J. Appl. Earth Obs. Geoinf.* **2012**, *14*, 112–128. [CrossRef]
7. Dai, J.; Zhao, L.; Jiang, Q.; Wang, H.; Liu, T. Review of thermal-infrared spectroscopy applied in geological ore exploration. *Acta Geol. Sin.* **2020**, *94*, 2520–2533.
8. Christensen, P.; Bandfield, J.; Hamilton, V.; Howard, D.; Lane, M.; Piatek, J.; Ruff, S.; Stefanov, W. A thermal emission spectral library of rock-forming minerals. *J. Geophys. Res. Planets* **2000**, *105*, 9735–9739. [CrossRef]
9. Baldridge, A.; Hook, S.; Grove, C.; Rivera, G. The ASTER spectral library version 2.0. *Remote Sens. Environ.* **2009**, *113*, 711–715. [CrossRef]
10. Hueni, A.; Nieke, J.; Schopfer, J.; Kneubühler, M.; Itten, K. The spectral database SPECCHIO for improved long-term usability and data sharing. *Comput. Geosci.* **2009**, *35*, 557–565. [CrossRef]
11. Xie, B.; Wu, L.; Mao, W.; Zhou, S.; Liu, S. An Open Integrated Rock Spectral Library (RockSL) for a Global Sharing and Matching Service. *Minerals* **2022**, *12*, 118. [CrossRef]
12. Govil, H.; Gill, N.; Rajendran, S.; Santosh, M.; Kumar, S. Identification of new base metal mineralization in Kumaon Himalaya, India, using hyperspectral remote sensing and hydrothermal alteration. *Ore Geol. Rev.* **2018**, *92*, 271–283. [CrossRef]
13. Rezaei, A.; Hassani, H.; Moarefvand, P.; Golmohammadi, A. Lithological mapping in Sangan region in Northeast Iran using ASTER satellite data and image processing methods. *Geol. Ecol. Landsc.* **2020**, *4*, 59–70. [CrossRef]
14. Loughlin, W. Principal component analysis for alteration mapping. *Proc. Themat. Conf. Geol. Remote Sens.* **1991**, *8*, 293–306.
15. Rokos, D.; Argialas, D.; Mavrantza, R.; Seymour, K.; Vamvoukakis, C.; Kouli, M.; Lamera, S.; Paraskevas, H.; Karfakis, I.; Denes, G. Structural Analysis for Gold Mineralization Using Remote Sensing and Geochemical Techniques in a GIS Environment: Island of Lesvos, Hellas. *Nat. Resour. Res.* **2000**, *9*, 277–293. [CrossRef]
16. Xie, M.; Zhang, Q.; Chen, S.; Li, Y.; Cha, F. Extraction of Alteration Anomaly Information by Feature-Based Principal Component Analysis from ASTER Data. *Earth Sci.—J. China Univ. Geosci.* **2015**, *40*, 1381–1385.
17. Liu, B.; Bai, S.; Yu, P.; Chen, M.; Pan, J.; Chen, Y. Land use analysis of plateau lake watershed based on GF and multi-source data. *Bull. Surv. Mapp.* **2019**, *12*, 77–82.
18. Li, W.; Liu, J.; Bao, N.; Mao, X.; Mao, Y.; Fu, Y.; Cao, W.; Huang, J.; Zhao, Z. Salinity Monitoring at Saline Sites with Visible–Near-Infrared Spectral Data. *Minerals* **2021**, *11*, 1086. [CrossRef]
19. Wang, D.; Liu, S.; Qi, Y.; Liu, H. Effect of Particle Size on Reflectance Spectra of Anshan Iron Ore. *Spectrosc. Spectr. Anal.* **2021**, *41*, 1513–1518.
20. Song, L.; Liu, S.; Yu, M.; Mao, Y.; Wu, L. A Classification Method Based on the Combination of Visible, Near-Infrared and Thermal Infrared Spectrum for Coal and Gangue Distinguishment. *Spectrosc. Spectr. Anal.* **2017**, *37*, 416–422.
21. Zhang, R.; Cao, H.; Zeng, M.; Zhang, D.; Li, G. Scientific belt lithologic mapping based on ASTER spectral analysis: A case study from the Tashkorgan area (Xinjiang, China). *Acta Petrol. Sin.* **2016**, *32*, 3835–3846.

22. Neal, L.; Wilkinson, J.; Mason, P.; Chang, Z. Spectral characteristics of propylitic alteration minerals as a vectoring tool for porphyry copper deposits. *J. Geochem. Explor.* **2018**, *184*, 179–198. [CrossRef]
23. Lypaczewski, P.; Rivard, B. Estimating the Mg# and AlVI content of biotite and chlorite from shortwave infrared reflectance spectroscopy: Predictive equations and recommendations for their use. *Int. J. Appl. Earth Obs. Geoinf.* **2018**, *68*, 116–126.
24. Lin, D.; Tang, S.; Xi, Z.; Zhang, B. Geochemical Characteristics of Late Ordovician Shales in the Upper Yangtze Platform, South China: Implications for Redox Environmental Evolution. *Minerals* **2021**, *11*, 710. [CrossRef]
25. Li, J.; Guo, J.; Wang, Z.; Wang, Z.; Liu, C. Geological characteristics of organic-rich shale in Yanxi formation of middle Ordovician in central Hunan. *J. Cent. South Univ. Sci. Technol.* **2018**, *49*, 2776–2786.
26. Fisenko, A.; Lemberg, V. Polylogarithmic Representation of Radiative and Thermodynamic Properties of Thermal Radiation in a Given Spectral Range: II. Real-Body Radiation. *Int. J. Thermophys.* **2015**, *36*, 2705–2719. [CrossRef]
27. Clark, R.; King, T.; Gorelick, N. Automatic continuum analysis of reflectance spectra. In Proceedings of the 3rd Airborne Imaging Spectrometer Data Analysis Workshop, Pasadena, CA, USA, 2–4 June 1987.
28. Crosta, A.; Moore, J. Enhancement of Landsat Thematic Mapper imagery for residual soil mapping in SW Minais Gerais State, Brazil: A prospecting case history in Greenstone belt terrain. In Proceedings of the 7th Thematic Conference on Remote Sensing for Exploration Geology, Calgary, AB, Canada, 2–6 October 1989.
29. Li, R. *Crystallography and Mineralogy*; Geology Press: Beijing, China, 2008.
30. Salisbury, J.; Aria, D. Emissivity of terrestrial materials in the 8–14 μm atmospheric window. *Remote Sens. Environ.* **1992**, *42*, 83–106. [CrossRef]